Multiferroic perovskites under epitaxial strain

Daumont, Cristophe

Chapter 4

Magnetic and electronic properties of $TbMnO_3$ films on (001)-$SrTiO_3$

4.1 Abstract

In this chapter we show that, unlike the bulk material, the $TbMnO_3$ films display ferromagnetic interactions below the antiferromagnetic ordering temperature of $T_N \sim 40K$. Moreover, x-ray photoemission measurements in the films show that the Mn-3s splitting is 0.3 eV larger than that of the bulk. *Ab initio* embedded cluster calculations yield Mn-3s splittings that are in agreement with the experiment and reveal that the larger observed values are due to a larger ionicity of the strained films. The origin of the observed ferromagnetism is investigated. We have found strong indications that the ferromagnetism originates at the walls between crystallographic (antiferromagnetic) domains. However, induced ferromagnetism due to the decrease of orthorhombic distortion cannot be totally excluded.

4.2 Introduction

(001)-oriented $TbMnO_3$ thin films were deposited on atomically flat TiO_2-terminated (001)-$SrTiO_3$ cubic substrates by Pulsed Laser Deposition. The deposition was performed at a substrate temperature of 750^oC and at oxygen pressures of 0.25 and 0.9 mbar. Structural characterization, including high resolution synchrotron and lab diffrac-

tometer x-ray measurements, showed that the thin films grow under compressive strain and have a distorted orthorhombic perovskite structure with the [001] orientation and free from secondary phases. The thin films are clamped to the substrate along one of the in-plane [100]-directions, while they maintain an orthorhombic structure that evolves with thickness (with the orthorhombic distortion decreasing for decreasing thickness, reaching the tetragonal phase for ultra thin films of 2 nm). Four equivalent orientational crystallographic domains, all with the c-axis out of plane, are present so the films keep the four-fold macroscopic symmetry of the substrate.

4.3 Results

4.3.1 Magnetic properties of the $TbMnO_3$ thin films grown at 0.9mbar

Figure 4.1 shows the magnetic moment as a function of temperature for a 30nm TMO film grown at 0.9mbar, measured under zero-field-cooling (ZFC) and field-cooling (FC) conditions. The magnetization presents an up-turn at T*$\sim$40K, indicative of a magnetic phase transition. We notice that this transition is very close to the magnetic ordering temperature ($T_N \sim$40K), from the paramagnetic phase to the sinusoidal antiferromagnetic structure of the manganese spins, observed in the bulk compound. This transition is then likely to also be associated to the manganese spins ordering. Another transition is observed at around $\sim$10K, also present in bulk $TbMnO_3$, which can be associated to the terbium spin ordering.

Other features can be observed in this measurement: A splitting at low temperatures between FC and ZFC measurements can be seen below the manganese spin ordering temperature. This indicates that ferromagnetic interactions are present in the films. The films then behave differently from the bulk form of $TbMnO_3$, which does not display FC-ZFC hysteresis. The magnetic measurements did not reveal any feature related to the stabilization of the spiral antiferromagnetic ordering -concomitant with the onset of ferroelectricity- which occurs in bulk at $\sim$27K. However, due to the

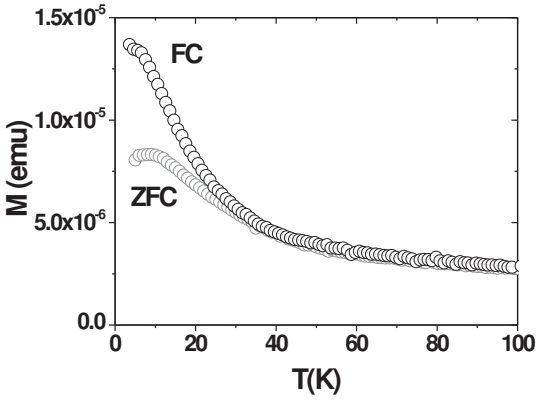

Figure 4.1: *Magnetic moment (M) as a function of temperature (T) for a 30nm TMO film grown at 0.9mbar. Data were recorded upon warming, with a 500 Oe field applied parallel to the film's surface. The diamagnetic contribution arising from the STO substrate was measured in a separate control experiment and subtracted from the raw magnetization.*

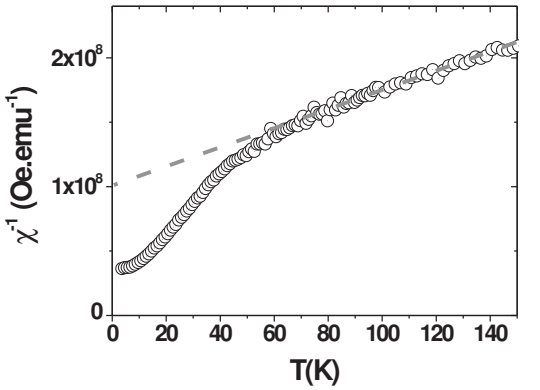

Figure 4.2: *Inverse susceptibility (χ^{-1}) as a function of temperature for a 30nm $TbMnO_3$ film grown at 0,9mbar.*

small sample volume and the substrate contributions, small anomalies in the magnetic susceptibility (as the one expected at the spin spiral transition) may be difficult to observe when measuring thin films. Moreover, one has to be very careful with the interpretation of magnetic measurements in thin films, where small amounts of magnetic impurity, often associated with the thick substrate, can provide a magnetization comparable to that of the films.

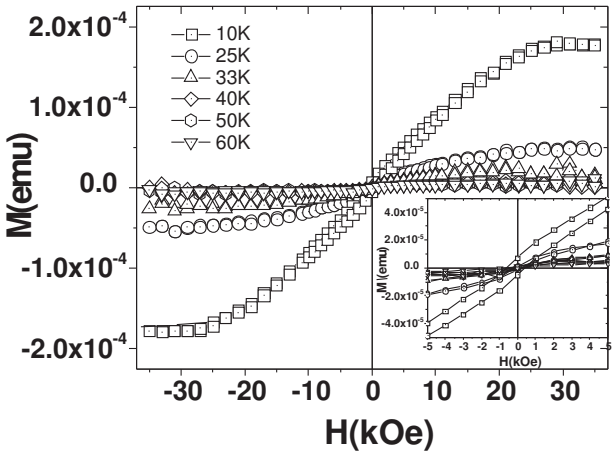

Figure 4.3: *Magnetic moment versus applied magnetic field at different temperatures ranging from 10K to 60K for a 30nm $TbMnO_3$ film grown at 0.9mbar. Both the diamagnetism of the substrate and the paramagnetism of Tb-ions have been deducted from the raw data.*

The deviation from the Curie-Weiss behaviour can be better appreciated in the evolution of the inverse susceptibility (χ^{-1}) with temperature (figure 4.2), where a change of slope can be seen at T*, consistent with a ferromagnetic contribution. The modeling of the high temperature tail of figure 4.2 by means of a Curie-Weiss law gives a negative extrapolated temperature ($\theta_{CW} \sim$ -150K), indicating that the dominant magnetic interactions are antiferromagnetic. Figure 4.3 shows magnetization loops measured at different temperatures from 10K to 60K and under applied magnetic fields ranging from -4T to 4T. From these loops, the saturation magnetization (M_S) is extracted. Figure 4.4 depicts the evolution of M_S with temperature, showing that ferromagnetic interactions develop below T*$\sim$40K. Since the maximum saturation magnetization is only 1.5 μ_B/fu, we can say that the character of the transition is ferrimagnetic-like. Similar effects have recently been observed in orthorhombic $YMnO_3$ and $YbMnO_3$ thin films [73, 75], as discussed in the introduction, which could suggest a general mechanism for induced ferromagnetism in manganite thin films.

Special attention should be paid to the possible existence of Mn_3O_4 impurities, which are ferrimagnetic with a T_C of 44K [105](even though we were unable to observe them by x-ray diffraction), and which could account for the presence of ferro-

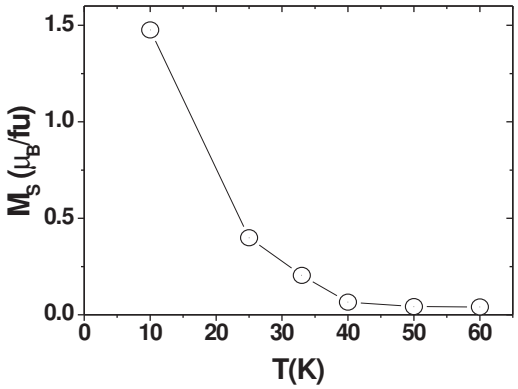

Figure 4.4: *Saturation magnetization (M_S) as a function of temperature for a 30nm $TbMnO_3$ film grown at 0.9mbar*

magnetism at low temperatures. However, that would imply a too large amount of Mn_3O_4 present in the films, which would have been detected by x-ray diffraction.

4.3.2 Effect of oxygen pressure during growth on the magnetic properties of $TbMnO_3$

The magnetic characterization corresponding to films grown at very different oxygen pressures (and different thicknesses, as will be discussed later) displayed qualitatively analogous results, as shown for a 100nm film grown at 0.25mbar and measured under the same conditions as the film grown at 0.9mbar, in figure 4.5. This indicates that the induced ferromagnetic moment in the films is not due to oxygen vacancies giving rise to a mixed-valence state. Indeed, a mixed valence state in the films can give rise to ferromagnetism mediated via the double exchange mechanism, common in doped manganites. According to our results, the oxygen pressure during deposition does not have a crucial role on the qualitative magnetic behavior of the thin films, for the investigated pressures.

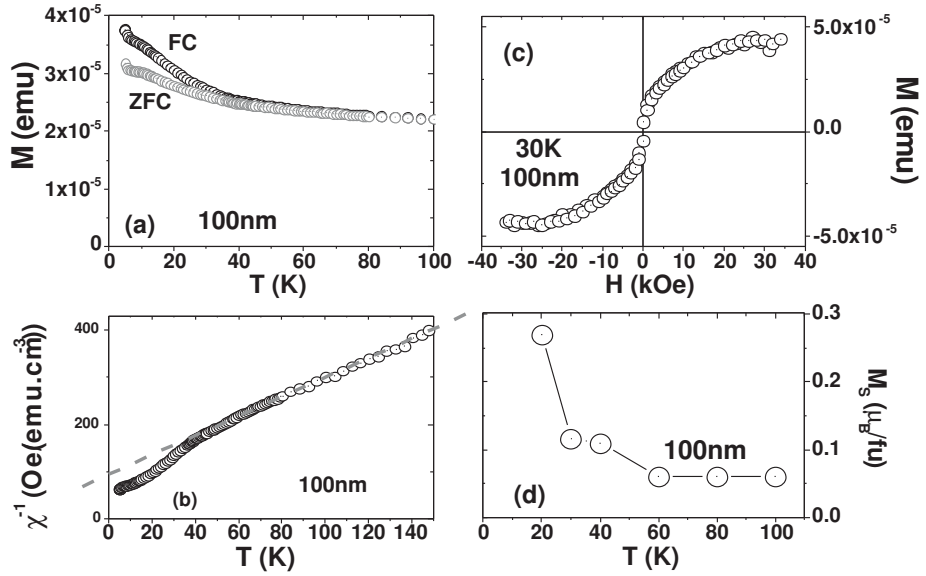

Figure 4.5: *(a) Magnetization (M) as a function of temperature (T) for a 100nm $TbMnO_3$ film grown at 0.25mbar. (b) Inverse susceptibility (χ^{-1}) as a function of temperature for the same film. (c) Magnetization versus magnetic field (H) at a temperature of 30K. (d) Saturation magnetization (M_S) as a function of temperature.*

4.3.3 Electronic properties of the $TbMnO_3$ thin films

In order to learn about the stoichiometry of the films, the oxidation state of manganese has been investigated. It is generally expected that oxygen content variations lead to a mixed valence state of the manganese in the system (Mn^{2+}/Mn^{3+} for oxygen vacancies [106, 107] and Mn^{3+}/Mn^{4+} for oxygen excess [106, 108]). XPS is a powerful tool to investigate the surface chemistry [109, 110]. The manganese Mn3s core level exhibits an exchange splitting characterized by two peaks in the XPS spectra. These peaks originate from the exchange coupling between the 3s hole and the 3d electrons [109]. A splitting of the manganese Mn3s core level of ΔE_{ex}=5-5.3 eV is expected for a nominal +3 valence. A decrease in the splitting is associated to a mixed +3/+4 valence state, whereas an increase of the splitting typically implies a mixed +2/+3 valence state. Even though the study of the Mn2p core level is not an easy task, due to the deconvolution of this core level into multiplets [111–113], the manganese Mn2p level exhibits also typical features depending on the valence state of the manganese. For +2 valence , a clear shake-up satellite can be seen at a binding energy of 647 eV, with a position of the

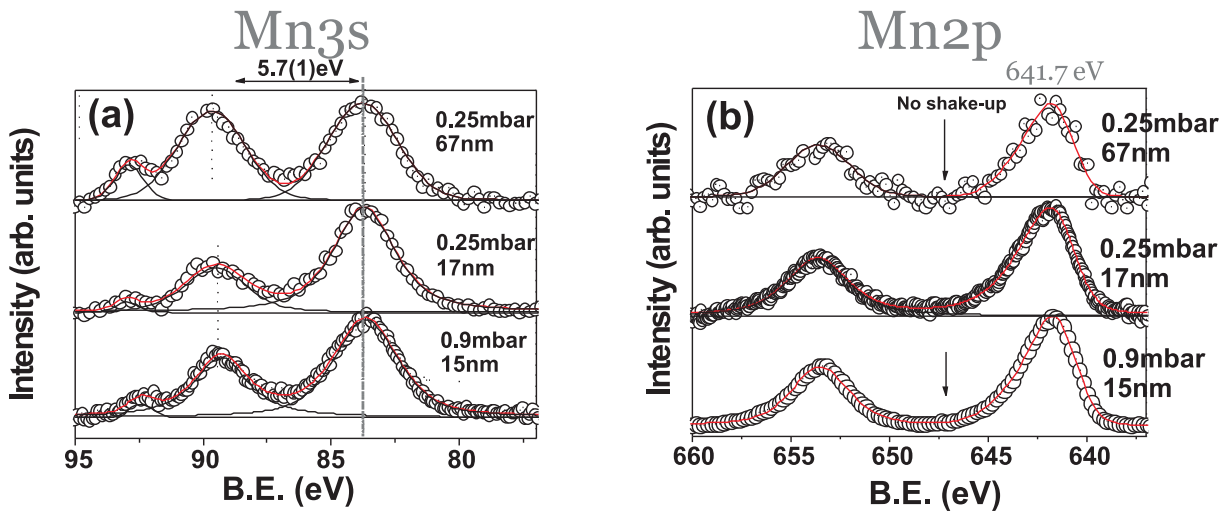

Figure 4.6: *(a) and (b) XPS spectra at the Mn3s and Mn2p core shells, respectively, $TbMnO_3$ films grown at pO_2= 0.25mbar and 0.9mbar for two different thicknesses. The lines are the fit to the peaks with gaussian profiles (two for the peak at 641.7 eV) after background subtraction (using the Shirley function).*

main peak around 640.8 eV. A valence of +3 exhibits a peak at a binding energy of 641.7 eV. Finally, a valence of +4 exhibits a peak at a binding energy of 642.8 eV. Moreover, the Mn2p peaks present a constant splitting of around 11.8eV [106, 114–116].

Figure 4.6 (a) shows the XPS spectra around the Mn3s core shell for films grown at 0.25mbar and 0.9mbar, for two different thickness. A splitting of the Mn3s core level of ΔE_{ex}=5.7(1)eV is found in our films, whose position does not change with thickness or oxygen pressure during growth. A third small peak can be seen at binding energies of around 93 eV, whose origin remains unclear. At first inspection, the splitting of 5.7 eV seems to indicate that the manganese in our films has a mixed +2/+3 valence and possibly oxygen vacancies. However, the splitting between the two Mn2p peaks, shown in Figure 4.6 (b), is Δ= 11.7eV, consistent with that expected for Mn^{3+}. Post annealing at very high oxygen pressures was done and no change in the splitting could be found. In addition, the Mn2p core level shows no shake-up satellites typical for the presence of Mn^{2+}. The low binding energy peak is found to be at 641.8 eV, also consistent with a nominal Mn valence of +3. No significant changes in the splitting are observed in the XPS spectra of the films grown with an oxygen pressure of 0.9mbar, and shown in

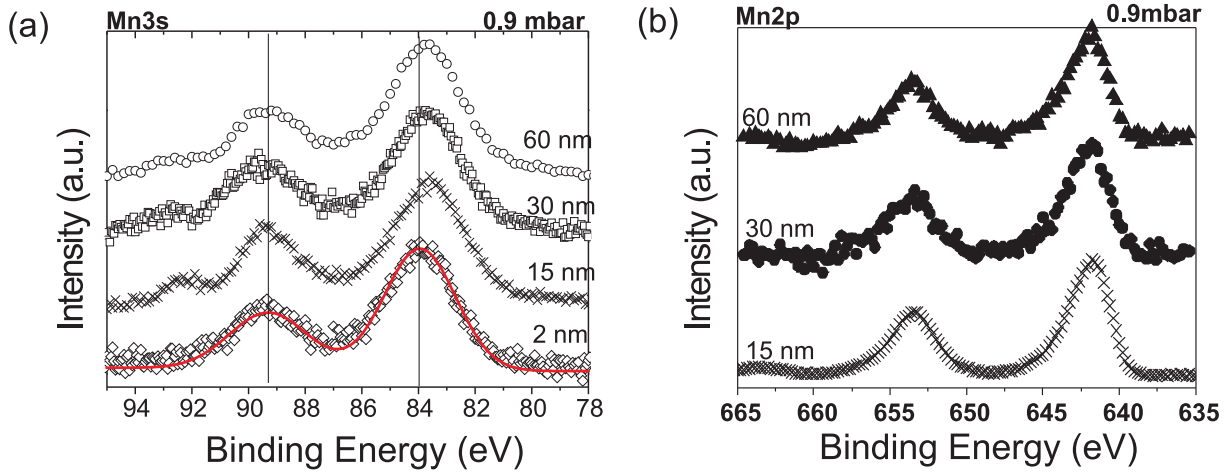

Figure 4.7: *XPS spectra at the Mn3s (a) and Mn2p (b) core shells, respectively, for $TbMnO_3$ films grown at pO_2=0.9mbar for different thicknesses. The line is a fit to the data after substraction of the background using the Shirley function. For clarity, only the Mn3s spectra is shown for the 2nm TMO film.*

Figure 4.6.

Thus, the comparison of the different XPS spectra leads to what appears to be contradictory conclusions: Irrespective of the oxygen pressure during growth or the thickness of the films, the relative large splitting in the Mn3s spectra indicate a mixed +2/+3 valence state of the manganese. However, looking at the Mn2p core levels of the same samples we find no indication of the shake-up peak associated with the Mn^{2+} valence. Moreover, the position of the low energy peak of this region agrees perfectly with the position of the manganese in a +3 valence state. In the next section, we will show that the increase in the splitting is due to a larger ionicity in the films. This strongly suggests that our films are stoichiometric and that the observed magnetization is not arising from a mixed valence that leads to the double-exchange mechanism [117].

The intensity of the peak with a binding energy of 93 eV, observed in our films, (see also figure 4.6 (a)) seems to be associated with the asymmetry and the intensity change observed for the peak at ≈89eV. The origin of this effect is unclear. It is worth to mention that the extra peak is absent in the fully strained and tetragonal (domain free) 2nm film (figure 4.7 (a)).

In order to shed light into the origin of the increased Mn3s splitting, configuration

interaction (CI) calculations[1] were performed, within the embedded cluster approach [118].

4.3.4 Cluster calculations

The electronic structure of an MnO_6 cluster is calculated with accurate quantum chemical schemes that ensure a precise and unbiased treatment of the strong electron correlation effects present in this type of materials. This MnO_6 cluster is embedded in a set of point charges that reproduce the Madelung potential in the cluster region due to the rest of the crystal. To avoid an artificial delocalization of the cluster electrons to the point charges, the centers nearest to the cluster are represented with model potentials [119] that account for the Coulomb and exchange interactions between the electrons in the cluster and the surroundings. This local approach has been successfully applied in the past to interpret XPS spectra of various ionic TM oxides [120, 121].

The final states responsible for the two peaks in the Mn3s XPS spectrum are characterized by a $3s^1 3p^6 3d^5$ electronic configuration. Only taking into account this configuration, very large exchange splittings are obtained in the calculations. However, it was shown by Bagus and collaborators [122] in the analysis of the exchange splitting in MnO that important contributions to the wave function arise from $3s^2 3p^4 3d^6$ electronic configurations. Semi-quantitative agreement with experiment can be obtained by also including the $3s^2 3p^5 3d^4 4f^1$ configurations. Applying this strategy to embedded MnO_6 clusters representing MnO, $LaMnO_3$ and $CaMnO_3$ give exchange splittings of 6.38, 5.72 and 3.95 eV, respectively. These calculated values are in good agreement with the experimental numbers: 6.2 eV for MnO; 5.3 eV for $LaMnO_3$ and 4.0 eV for $CaMnO_3$.

The embedded cluster for bulk $TbMnO_3$ was constructed using the experimental structure [39]. For the thin film cluster, we applied the lattice parameters of a 8nm film.

[1] These calculations, detailed in the next subsection, were performed by our collaborators Coen de Graaf (Department of Physical and Inorganic Chemistry, Tarragona, Spain) and Ria Broer (Theoretical Chemistry group, Zernike Institute for Advanced Materials, University of Groningen).

The CI calculations give an exchange splitting of 5.18 eV for bulk $TbMnO_3$ and 5.46 eV for the thin film. The slight underestimation in comparison to the experimental value of 5.7 eV reported in Fig. 4(a) is to be expected because in the calculations the 4f type expansion functions were not optimized. The increase of +0.3 eV in comparison to bulk is precisely what is observed in the experiment.

The steady increase of the exchange splitting from $CaMnO_3$ to $LaMnO_3$ to MnO suggests that the exchange splitting is determined by the formal ionic Mn charge as reported by Galakhov [123]. However, this relationship cannot be used to explain the different exchange splitting in bulk and thin film $TbMnO_3$, since in both cases the formal Mn charge is the same. Actually the calculated Mn charge is slightly smaller in the bulk than in the thin film contradicting the suggested relationship between Mn charge and exchange splitting. Serious doubts have been raised on the usefulness of the concept of the formal charge and/or oxidation state to interpret the electronic structure of transition metal compounds [124, 125]. Instead, we analyze the relation between the exchange splitting and the screening of the core hole by the oxygen ligands. For this purpose, the N-electron wave function is expressed in localized orbitals [118] and configurations are grouped by non charge transfer (Mn-$3d^5$), charge transfer (Mn-$3d^6L^{-1}$) and configurations with two or more electrons transferred from oxygen to Mn. This analysis shows that the screening of the core hole by the oxygens is more effective in the bulk than in the film; the charge transfer (CT) configurations have a larger weight in the wave function of the bulk cluster (44%) than in the film (38%). Hence, instead of the formal Mn charge, the exchange splitting is determined by the degree of oxygen screening. It is well known that MnO is highly ionic with almost no charge transfer in the wave function, while $CaMnO_3$ has a more covalent character with a much larger degree of screening, in line with the observed exchange splittings.

The reduced degree of core hole screening by the oxygens in the films is related to the shorter Mn-O distances in the ab-plane (Note that the Mn-O distance were extracted considering bulk atomic positions for the atoms considered). These shorter distances make that the oxygen-to-metal charge transfer configuration lies higher in

energy and contributes less to the wave function. In a one-electron reasoning this can be explained by the fact that shorter Mn-O distances lead to enhanced anti-bonding interactions, which increase the Mn-3d orbital energies. This causes a higher charge transfer energy, and hence, less effective ligand screening.

4.4 Discussion: Possible origins of ferromagnetism

With the previous study we rule out the double exchange mechanism between different Mn ions as the origin of the observed ferromagnetism. It is tempting to say that the decreased charge transfer in the films established previously, reduces the efficiency of the superexchange mechanism and enhances ferromagnetism with respect to the bulk case, in agreement with our experimental observations. However, given the subtle competition between ferromagnetic and antiferromagnetic exchange constants in this material [67] and the likely influence of the Tb ions, a more complex analysis of the magnetic structure of the films is needed. Strain can also have tremendous effects on orbital ordering [126], which determines the magnetic properties of $TbMnO_3$. To elucidate these possibilities, the full structure determination of the films, including the oxygen atomic positions, is compulsory but not technically possible at the present time.

Another possible origin of the observed ferromagnetism is the direct coupling between magnetization and strain. In this respect, there is an analogy between the induction of ferromagnetism in epitaxial antiferromagnets and the well-known induced ferroelectricity in incipient ferroelectrics [127, 128]. The strong coupling of the magnetic structure of $TbMnO_3$ to the lattice has been recently demonstrated [129]. The epitaxial stress in the films is estimated to be $2x10^8$ N/m^2, using a value of the Young modulus of 20 GPa [130] and, thus, the magnetization values observed are compatible with an effective piezomagnetic coefficient (linear part of the magnetostriction) of 10^{-10} m/A. This value is substantially smaller than the reported magnetostriction val-

ues in the bulk [129]. However, the presence of in-plane domains in the films makes it difficult to extract any final conclusions.

Finally, the origin of ferromagnetism could be in the microstructure. The TEM images shown in the previous chapter reveal that the size of the orthorhombic domains decreases for decreasing thickness and, thus, that the thinner the films, the larger the volume ratio of domain walls present. This is most relevant in order to understand the physical properties observed in the films, that is the induced ferromagnetism, and the absence of a lock-in transition. Although the orthorhombic domains of the bulk material are known to be antiferromagnetic in character, also in agreement with the negative Curie-Weiss temperature measured in the films, the interactions at the crystallographic domain walls could give rise to the observed ferromagnetic component. Moreover, the long range order of the spin cycloid that gives rise to the lock-in and ferroelectric transition, is disturbed by the presence of crystallographic domain walls/boundaries, which precludes the appearance of long range order and macroscopic polarization, consistent with our observations.

4.5 Thickness dependence of induced ferromagnetism

As stated above, the domain structure, characterized by XRD and clearly imaged by TEM (see Chapter 3) might be at the origin of the induced ferromagnetism. However, magnetostriction or another (indirect) effect of strain cannot be ruled out completely. Fortunately, as shown in Chapter 3, the strain state in the films is constant up to a thickness of about 70nm, while the density of domain walls increases linearly with decreasing thickness. So the evolution of the magnitude of the FC-ZFC splitting in the magnetization with thickness can help us narrow down the causes of ferromagnetism in our films.

Figure 4.8 shows the evolution of the magnetization of $TbMnO_3$ thin films with thicknesses ranging from 15nm to 80nm under zero-field-cooled (full symbols) and

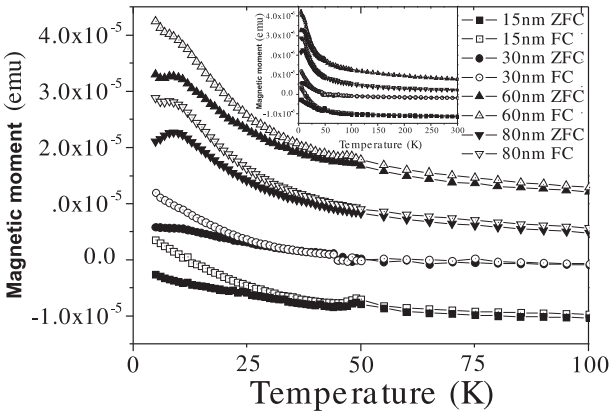

Figure 4.8: *Evolution of the magnetic moment, under zero-field-cooled (full symbols) and field-cooled (open symbols) conditions, as a function of thickness for the films grown at 0.9mbar. The inset shows the data up to 300K.*

field-cooled (open symbols) for temperatures ranging from 5K to 100K (the inset shows the data up to 300K).

For clarity, the raw data are presented. An unexpected small splitting at all the temperatures for all the samples can be observed (see inset of figure 4.8). This can be due to the shift of the sample during the field cooling due to the applied field or to ferromagnetic impurities with $T_c \geq 300$K, not relevant for the discussion. Due to the small response of the thin films, we are sensitive to small motion of the samples (same measurements repeated with a different sample mounting, resulting in a different splitting). This splitting at high temperatures is taken into account as the error bars in figure 4.10. This can not be explained by the substrate contribution, as it was measured to be negative ($SrTiO_3$ is diamagnetic) under this applied magnetic field (see figure 4.9).

To correctly take into account the substrate contribution is, indeed, a serious problem, since the $SrTiO_3$ substrates are known to contain impurities and different substrates show slightly different temperature dependence characteristics, specially at low temperatures. This small differences are critical in the case of the very thin films. The diffusion of silver paint (used to glue the substrate during growth and polished away after growth) into the $SrTiO_3$ cannot explain the extra magnetization at high tem-

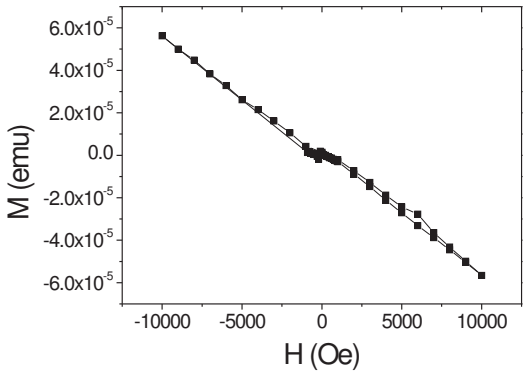

Figure 4.9: *Magnetic moment as a function of applied field for a bare $SrTiO_3$ substrate. The data were taken at 15K. $SrTiO_3$ is diamagnetic.*

peratures as it is also diamagnetic [131]. However, it can explain why the thinner films display a negative magnetization due to the bigger effect of the diamagnetic contribution from the substrate.

In order to extract the value of the FC-ZFC splitting, all the films were measured under an applied field of 1 kOe. The splitting was not measured at the minimum temperature but at 15 K instead, since at lower temperatures there is a change in behaviour with thickness, as the flattening due to the Tb ordering transition seems to be absent for the thinner films. Moreover, the paramagnetic contributions due to substrate impurities are smaller at higher temperatures. Figure 4.10 shows the evolution of the splitting between the ZFC and FC magnetization taken at 15K, normalized to the volume of the films. A decrease in the splitting with increasing thickness can be seen, from around 9 emu/cm^3, for the 15nm film, down to around 3 emu/cm^3 at 60nm. As shown in figure 4.10, there is a linear dependence of the splitting between the ZFC and FC curves with the inverse of the thickness for the films thinner than 80nm, those that are strained.

The induced magnetism shows the same thickness dependence as that of the density of domain walls, described in the previous chapter (see figure 3.16 in Chapter 3). For the thinner films, the crystallographic domains are found to be very small.

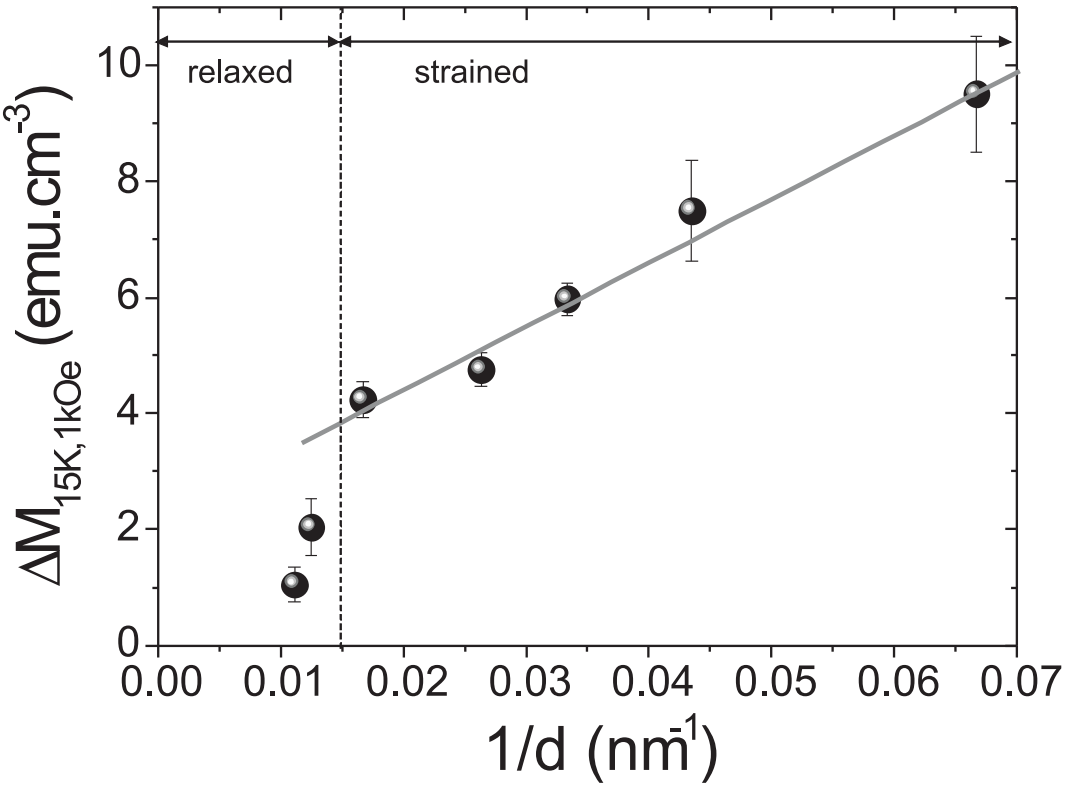

Figure 4.10: *Evolution of the splitting, between the zero-field-cooled and field-cooled magnetization, as a function of the inverse thickness, for the films grown at 0.9mbar. The error bars represent the value of the high-temperature splitting. The data have been normalized to the volume.*

This means that in the thin films the volume fraction of domain walls is very significant, and therefore the properties of the domain walls are likely to affect the overall magnetic properties. As the thickness is increased, the number of domain walls decreases, and therefore, also the magnetic response associated to them. The fact that the number of domain walls per unit area follows the same trend as the ZFC-FC splitting strongly suggests that the ferromagnetic interactions present in the film originate at the domain walls.

We turn now to check the effect of the orthorhombic distortion. As shown in Chapter 3, this can be measured by means of the pseudo-cubic angle, γ. Figure 4.11 plots γ as a function of the inverse of the thickness, also showing a linear behavior for the strained films. The orthorhombic distortion for the relaxed part of the thickest film,

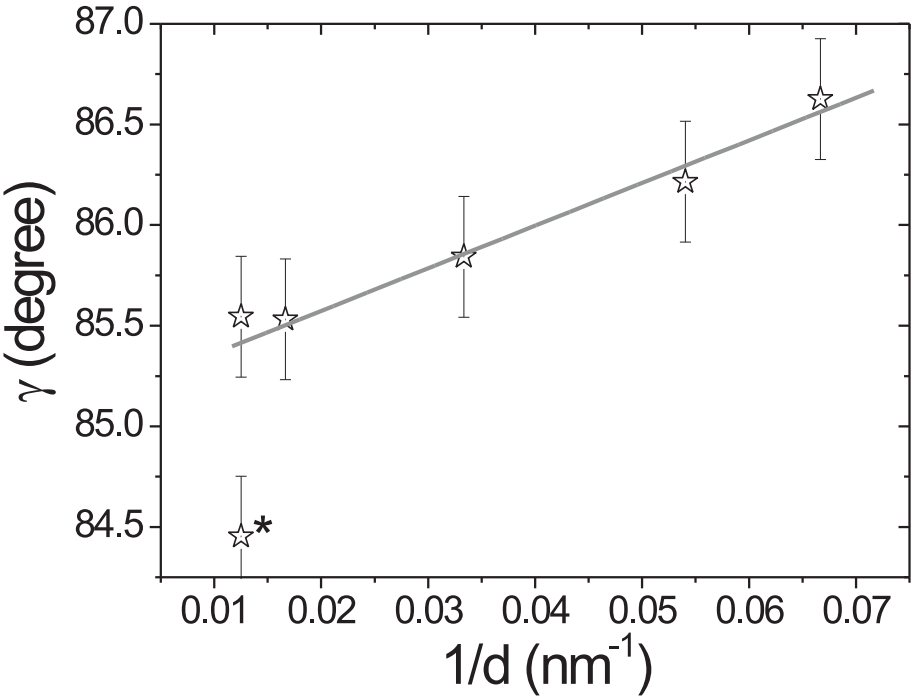

Figure 4.11: *Evolution of the orthorhombic distortion angle, γ, as a function of the inverse thickness for the samples grown at 0.9mbar. The black star indicates the value corresponding to the relaxed part of the film, which agrees with the bulk value.*

γ=84.4^o coincides with the reported bulk value. For the strained part present in the thickest film, the orthorhombic distortion saturates at a value of 85.5^o.

According to a very recent theoretical work, a decrease of orthorhombic distortion would modify the balance between the different competing exchange constants, increasing the ferromagnetic interactions [132]. This theoretical work of Dong $et\ al.$, which is a sequel of the microscopic model reproducing the cycloid phase in $TbMnO_3$ and $DyMnO_3$, discusses the possible ferromagnetism in manganites [132]. The calculations reproduce the different phases in manganites, including $TbMnO_3$. The hamiltonian used follows their previous work on manganites, and is expressed as:

$$H = H_{DE} + H_{AF} + H_{J2} + H_{JT} \tag{4.1}$$

where H_{DE} is the standard hamiltonian for double-exchange between e_g electrons, H_{AF} is the hamiltonian of the antiferromagnetic superexchange coupling between

nearest neighbours, H_{J2} is the nearest-next neighbour superexchange along the a and b axes and H_{JT} is sum of the hamiltonians of the electron-phonon coupling associated with the Jahn-Teller distortion and the energy of the Jahn-Teller distortion [132]. Although the standard double exchange associated to the hopping of e_g electrons between mixed valence ions is discarded (see previous section), Dong *et al.* can successfully reproduce the experimental phases by considering double exchange in undoped manganites. Using this model, the transition from an A-AFM to an E-AFM type magnetic structure has been reproduced as well as the intermediate cycloid state. The key point in the calculation is the appearance of a ferromagnetic phase when the model is extended to a three-dimensional infinite cubic lattice and the Jahn-Teller distortion is 'switched off'. As the Mn-O-Mn bond angle gets closer to 180^o degrees, the ratio between the double exchange and superexchange terms, will be enhanced, increasing the ferromagnetic tendency [132]. Moreover, the orthorhombic distortion stabilizes the $d_{3x^2-r^2}/d_{3y^2-r^2}$ type of orbital ordering, which would be suppressed in the nearly cubic lattice [132]. The effect of 'switching on' the Jahn-Teller distortion in the calculation decreases the ferromagnetic region but still cannot account for a reasonable value for the wavevector of $DyMnO_3$ [132]. It seems, thus, that the decrease of the distortion due to strain can, in principle, not be discarded as the possible cause of the ferromagnetism in the films. We will investigate now this possibility.

However, measuring the out-of-plane magnetic moment of strained films also reveals a ZFC-FC splitting below around 40K, as shown in figure 4.12 for a 60nm (a) and for a 20nm (b) $TbMnO_3$ film grown both at 0.9mbar. Both films show the same qualitative behaviour and ferromagnetic interactions are also evidenced out-of-plane. This is again different from the bulk behaviour, where the planes are antiferromagnetically coupled along the c-direction (see Introduction).

This is also not expected according to Dong's model previously discussed, since along this direction, the distortion is unchanged and therefore an antiferromagnetic response is expected. The induced ferromagnetism in the films is, therefore, not constrained to the ab plane, strongly suggesting that the ferromagnetic interactions ob-

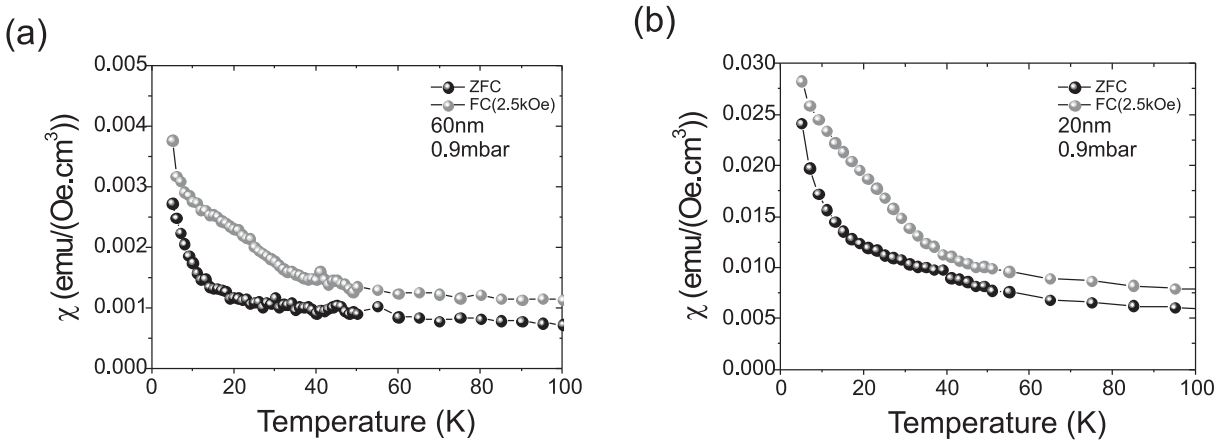

Figure 4.12: *(a) Zero-field-cooled (black circles) and field-cooled (grey circles) measurements of the magnetic susceptibility as a function of temperature for a 60nm $TbMnO_3$ film grown at 0.9mbar. (b) Zero-field-cooled (black circles) and field-cooled (grey circles) measurements of the magnetic susceptibility as a function of temperature for a 20nm $TbMnO_3$ film grown at 0.9mbar. The raw data are presented for clarity. In both measurements, the magnetic field was applied perpendicular to the surface of the films.*

served in the films are not directly related to the epitaxial strain, but instead to the presence of domain walls. The linear dependence of the orthorhombic distortion with the domain wall density is not coincidental since the size of the domains is directly related to the structural distortion [133]. Moreover, the fact that the observed splitting between the zero-field-cooled and field-cooled curves occurs at the bulk temperature of 40K, suggests that the bond angles are bulk-like and are not modified in the thin film form of $TbMnO_3$. However, the unfeasibility to refine the atomic positions and thus the bond distances and angles, makes any direct conclusion impossible at this stage.

If we assume that the crystallographic (and antiferromagnetic) domain walls are also ferroelectric (at least locally), that is they are multiferroic, we could naturally explain the ferromagnetic component: Symmetry arguments show that magnetoelectric coupling can induce ferromagnetism in the domain walls of ferroelectric antiferromagnets [134–136], and works by Fiebig and co-workers have also shown that the ferroelectric domain walls of multiferroic hexagonal manganites can have a net magnetization at their center [137] as well as enhanced magnetoelectric coupling [138, 139].

Recently, interesting properties have been observed in multiferroic domain walls in $BiFeO_3$ thin films, where conduction at the multiferroic domain wall was evidenced, pointing out the possible integration of such properties in devices at small scales [140, 141], as well as the peculiar properties of domain walls in magnetoelectric multiferroics. Knowing that the behaviour of the dielectric constant can also be affected by magnetic ordering, the measure of the dielectric constant is relevant in order to elucidate the origin of the induced ferromagentism and will be discussed in the next chapter.

4.6 Conclusions

In summary, $TbMnO_3$ films grown epitaxially on $SrTiO_3$ substrates display a strained orthorhombic perovskite structure less distorted than that of the bulk. This structural modification gives rise to an increased ionicity in the films with respect to the bulk. It has also been shown that the physical properties of these films are very different from those of the bulk: The films show ZFC-FC hysteresis below the N$\acute{e}$el temperature of $\sim 40K$, which is absent in the bulk. This can be of interest due to the scarcity of ferromagnetic insulators. Our data point towards the physical properties of the films being directly associated to the crystallographic domain walls, present in large quantities in the films: The investigation of the magnetic properties of the films as a function of thickness shows a linear increase of the splitting between the ZFC and FC, with decreasing thickness. The domain wall density follows the same trend, strongly indicating that the ferromagnetism originates at the walls. The fact that the orthorhombic distortion (pseudo-cubic angle) follows the same trend with thickness arises from the direct relationship betwen the domain size and the crystallographic distortion. The appearence of the induced ferromagnetism, both in the in-plane as well as in out-of-plane directions, strongly indicates that the induced ferromagnetism originates at the domain walls and is not directly caused by the epitaxial strain.